$(CuI)_2Cu_3SbS_3$: Copper Iodide as Solid Solvent for Thiometalate Ions

Arno Pfitzner*

Dedicated to Professor Hans Georg von Schnering

Abstract: $(CuI)_2Cu_3SbS_3$ was prepared by solid-state reaction of stoichiometric amounts of CuI, Cu, S, and Sb. The crystal structure was determined from single crystals at room temperature and $-80\,^{\circ}C$. Red-orange $(CuI)_2Cu_3SbS_3$ crystallizes in the orthorhombic system, space group *Pnnm* (no. 58) with $a = 10.488(2)$, $b = 12.619(2)$, $c = 7.316(1)$ Å, $V = 968.2(2)$ Å^3 (20 °C), and $Z = 4$. The distribution of the copper atoms was refined by using a Gram-Charlier nonharmonic development of their atomic displacement parameters, which indicated an increasing dynamic disorder from $-80\,^{\circ}C$ to $20\,^{\circ}C$. Raman spectra of $(CuI)_2Cu_3SbS_3$ are dominated by strong bands for $[SbS_3]^{3-}$ units at 362 and 338 cm^{-1}. The compound melts at 492 °C (DTA, onset). Conductivity measurements reveal high ionic conductivity ($6.2 \times 10^{-5}\,\Omega^{-1}\,cm^{-1}$ at 50 °C, $2.9 \times 10^{-3}\,\Omega^{-1}\,cm^{-1}$ at 200 °C) with an activation energy of 0.35 eV (40–275 °C).

Keywords antimony · chalcogens · copper · iodine · solid-state structures

Introduction

In the past two decades preparative solid-state chemistry has made considerable progress by the use of either reactive flux techniques or the well-known solventothermal synthesis route. Alkali metal chalcogenide systems[1] have proved particularly popular as flux media, and the solventothermal media employed have ranged from mineral acids[2] to organic solvents.[3] Recently copper(I) halides have been shown to be good solid solvents for numerous polymeric *neutral* or *low charged* main group molecules or anions, respectively. Thus, chalcogen chains $^1_\infty[Se^0]$, $^1_\infty[Te^0]$, $^1_\infty[SeTe^0]$, and $^1_\infty[STe^0]$,[4] or chalcogen rings $[Se_6^0]$, $[Se_{6-x}Te_x^0]$, and $[Se_{6-x}S_x^0]$[5] were obtained as copper(I) halide adducts. Several compounds could also be isolated in the copper(I) halide–phosphorus system such as the *neutral* polymers $^1_\infty[P_{12}^0]$ (two different types) and $^1_\infty[P_{14}^0]$ and *low charged* polyanions $^1_\infty[P_{15}^{-1}]$ and $^1_\infty[P_{20}^{-2}]$.[6] In all these compounds copper atoms are coordinated both to halide ions and to atoms of the polymeric chains of Group 15 or 16 elements. From the crystal structures it becomes evident that the preferred positions for coordination are the lone pairs of electrons on these atoms. Nevertheless, the bond lengths and angles in the main group polymers are not significantly influenced by surrounding copper atoms. Thus, it can be assumed that the structural flexibility of the copper halide matrix plays an important role for the three-dimensional arrangement of the polymers in the solid state. It may also act as a catalyst for the formation and help to stabilize the *neutral* or *low charged* molecular fragments.[6] The existence of $(CuI)_3Cu_2TeS_3$ shows that not only large polymeric molecules but also small anionic species, such as the $[TeS_3]^{2-}$ unit, can be obtained in a copper halide matrix.[7] In $(CuI)_3Cu_2TeS_3$ the thiometalate ions are separated from each other by the surrounding copper halide. In several cases the presence of a large number of energetically almost equivalent sites results in a pronounced disorder of copper atoms and a noticeable ionic conductivity. Thus, these compounds can be regarded as a new class of ionic conductors.[6] Herein the preparation, structural characterization, Raman spectroscopic properties, and ionic conductivity of $(CuI)_2Cu_3SbS_3$ are reported. This compound was previously reported as $Cu_5SbS_3I_2$ in a short note in which only the lattice constants but no additional information was provided.[8]

[*] Dr. A. Pfitzner
Anorganische Chemie
Universität-Gesamthochschule Siegen
D-57068 Siegen (Germany)
Fax: Int. code + (271)740-2555
e-mail: pfitzner@chemie.uni-siegen.d400.de

Results and Discussion

Crystal Structure: Crystallographic details of the structure determination of $(CuI)_2Cu_3SbS_3$ (Table 1) indicate that the compound crystallizes in the orthorhombic space group *Pnnm*. The ratio $b/c = 1.7227$ is close to $\sqrt{3}$, which might suggest that the cell is hexagonal, but the X-ray powder pattern shows numerous reflections that cannot be indexed by using the corresponding hexagonal cell. Table 2 contains the refined atomic coordinates and displacement parameters, Table 3a lists selected interatomic distances and angles. The arrangement of the I^- and $[SbS_3]^{3-}$ ions in the crystal structure of $(CuI)_2Cu_3SbS_3$ is shown in Figure 1. From a topological point of view the iodine part of the anionic substructure can be derived from the hexagonal diamond structure ($d(I-I) < 4.3$ Å). Thus, the iodide ions form an eutactic network of six-membered rings in chair and boat

  0947-6539/97/0312-2032 $ 17.50+.50/0

Table 1. Crystallographic data for $(CuI)_2Cu_3SbS_3$ [a].

T [°C]	20	−80
formula	$Cu_5SbI_2S_5$	
M [g mol^{-1}]	789.43	
space group, formula units	*Pnnm* (no. 58), $Z = 4$	
crystal dimensions [mm]	0.07 × 0.07 × 0.07	
lattice constants [Å] [b]: a	10.488(2)	10.531(3)
b	12.619(2)	12.609(3)
c	7.316(1)	7.278(1)
cell volume V [Å^3]	968.2(2)	966.4(4)
ρ_{calcd} [g cm^{-3}]	5.418	5.424
absorption coefficient $\mu(Mo_{K\alpha})$ [mm^{-1}]	20.49	20.52
diffractometer	NONIUS CAD4, $Mo_{K\alpha}$, $\lambda = 0.71073$ Å, graphite monochromator, scintillation counter	
scan type	ω scans	
absorption correction	ψ scans	
transmission ratio (max:min)	0.961:0.712	
scan range	$2\theta < 60°$	
range in *hkl*	$-14 \le h \le 14$	$0 \le h \le 14$
	$0 \le k \le 17$	$-17 \le k \le 17$
	$0 \le l \le 10$	$0 \le l \le 10$
measured reflections	3184	2938
independent reflections, R_{int}	1511, 0.0452	1501, 0.0405
reflections used	1211 ($I > 1\sigma(I)$)	1243 ($I > 2\sigma(I)$)
refined parameters	108	105
program used	JANA96 [9]	
final $R/wR(I_{obs})$	0.0378, 0.0606	0.0379, 0.0791
final R/wR(all reflections)	0.0647, 0.0651	0.0555, 0.0808
goodness-of-fit	1.45	1.96
extinction coefficient	0.068(5) [c]	0.067(7) [c]
largest diff. peak/hole [e Å^{-3}]	2.27/−2.83	2.71/−2.74

[a] Further details of the crystal structure investigations are available on request from the Fachinformationszentrum Karlsruhe, D-76344 Eggenstein-Leopoldshafen (Germany), on quoting the depository numbers CSD-406988 ($T = 20$ °C) and CSD-406989 ($T = -80$ °C). [b] Powder data (20 °C), single crystal data (−80 °C). [c] Isotropic secondary extinction correction, Type I, Lorentzian distribution [10].

conformation. Some of the iodine atoms are replaced by trigonal-pyramidal (pseudo-tetrahedral) $[SbS_3]^{3-}$ units. As a consequence I(2) has four iodine atoms as next nearest neighbors, whereas I(1) is surrounded only by three further iodine atoms. The pseudo-threefold axes of the $[SbS_3]^{3-}$ units are oriented parallel to [100]. Distorted empty S_6 octahedra are formed by two thioantimonate(III) ions around the origin and symmetry-related positions (Figure 2b). No additional sulfur atoms are found for antimony as next nearest neighbours. Similar to

Abstract in German: *$(CuI)_2Cu_3SbS_3$ wurde durch Festkörperreaktion stöchiometrischer Mengen von CuI, Cu, S und Sb erhalten. Die Kristallstruktur bei Raumtemperatur und −80 °C wurde an Einkristallen bestimmt. Rot-oranges $(CuI)_2Cu_3SbS_3$ kristallisiert orthorhombisch, Raumgruppe Pnnm (Nr. 58) mit $a = 10.488(2)$, $b = 12.619(2)$, $c = 7.316(1)$ Å, $V = 968.2(2)$ Å^3 (20 °C) und $Z = 4$. Die Verteilung der Kupferatome wurde mit einer Gram-Charlier Entwicklung der Auslenkungsparameter verfeinert und so wurde eine, mit steigender Temperatur zunehmende, dynamische Fehlordnung nachgewiesen. Ramanspektren von $(CuI)_2Cu_3SbS_3$ zeigen im wesentlichen die intensiven Banden der $[SbS_3]^{3-}$-Ionen bei 362 und 338 cm^{-1}. Die Verbindung schmilzt bei 492 °C (DTA, onset-Wert). Leitfähigkeitsmessungen belegen eine hohe Ionenleitfähigkeit ($6.2 \times 10^{-5}\ \Omega^{-1}\,cm^{-1}$ bei 50 °C, $2.9 \times 10^{-3}\ \Omega^{-1}\,cm^{-1}$ bei 200 °C) verbunden mit einer Aktivierungsenergie von 0.35 eV (40–275 °C).*

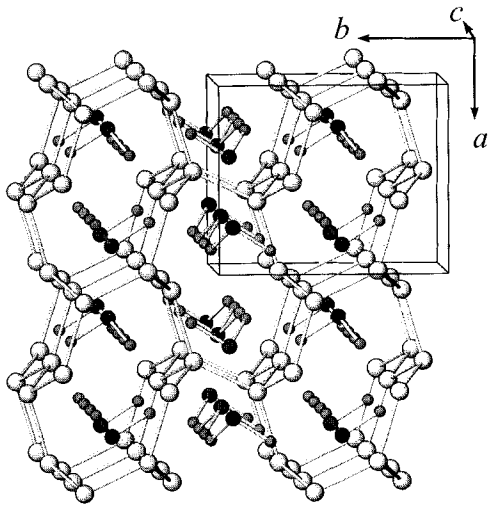

Figure 1. Section of the crystal structure of $(CuI)_2Cu_3SbS_3$ showing the arrangement of I^- and $[SbS_3]^{3-}$ ions (Cu atoms are omitted). Iodine atoms are connected to emphasize the relation of their eutactic packing to the hexagonal diamond structure. Sb: large dark spheres; S: small gray spheres; I: large light gray spheres.

$(CuI)_3Cu_2TeS_3$[7] the thiometalate ions can be regarded as isolated from each other in a copper iodide matrix.

Using the nonharmonic approach to describe the disorder of the copper atoms, four different positions are obtained for them. Two positions (Cu(1), Cu(2)) are fully occupied and two are occupied only to an extent of about 50% (Cu(3), Cu(4); see Table 2). Figure 2a shows a section of the crystal structure of $(CuI)_2Cu_3SbS_3$ parallel to (100). Cu(1) is located in a distorted tetrahedron comprising two sulfur and two iodine atoms. These tetrahedra are linked by common edges (I(1), I(2)) and common corners (S(1)), resulting in ribbons along [001]. A second ribbon built of only three-coordinate metal atoms—alternating Sb and Cu(2)—runs parallel to [001]. The coordination sphere of antimony consists exclusively of sulfur atoms, whereas Cu(2) has two sulfur atoms (S(2)) and one iodine atom (I(2)) as neighbors. For Cu(2) an additional iodine atom (I(1)) is observed at a distance of $d(Cu-I) \approx 3.4$ Å; this Cu atom is located in one face of a tetrahedron formed by two sulfur and two iodine atoms (cf. Figure 5c). The positions of Cu(3) and Cu(4) are only partly occupied; in the refinement their occupancy factors were constrained in such a way that the sum was equal to one. These atoms are located around the above-mentioned distorted S_6 octahedron. They are only distributed on those six faces of the octahedron that are not parallel to (100); electron density appropriate for the presence of a copper atom in the center of this octahedron is not observed. Taking distances smaller than 3 Å into account, Cu(3) is four-coordinate, surrounded by I(1), I(2), S(1), and S(2), whereas Cu(4) is coordinated exclusively by three sulfur atoms (S(1), 2 × S(2)).

Distribution of the Copper Atoms: The conventional (harmonic) refinement of the crystal structure at room temperature resulted in relatively large anisotropic displacement parameters of the copper atoms. In addition, eight positions with close neighbors and a refinement suffering from strong correlations were necessary to describe the distribution of copper. The anisotropic displacement parameters for copper deviate significantly from ideal (harmonic) behavior, which can be explained by a second-

  0947-6539/97/0312-2033 $ 17.50+.50/0

Table 2. Atomic coordinates and displacement parameters [Å^2] for $(CuI)_2Cu_3SbS_3$.

Atom	Wyckoff position	x	y	z	sof	U_{eq} [a]	U^{11}	U^{22}	U^{33}	U^{12}	U^{13}	U^{23}
					$T = 20\,^{\circ}C$							
I(1)	4g	0.55052(6)	0.26781(5)	0	1.0	0.0270(2)	0.0195(3)	0.0385(4)	0.0230(3)	0.0062(2)	0	0
I(2)	4g	0.08038(6)	0.63930(5)	0	1.0	0.0272(2)	0.0231(3)	0.0180(3)	0.0406(3)	0.0027(2)	0	0
Sb	4g	0.31098(5)	0.00751(5)	0	1.0	0.0207(2)	0.0124(2)	0.0201(3)	0.0296(3)	−0.0003(2)	0	0
S(1)	4g	0.1881(2)	0.1713(2)	0	1.0	0.0203(6)	0.0189(9)	0.0146(9)	0.0276(10)	−0.0007(8)	0	0
S(2)	8h	0.3168(1)	0.4248(1)	0.2595(2)	1.0	0.0205(4)	0.0222(7)	0.0204(7)	0.0191(7)	0.0027(6)	−0.0003(6)	−0.0024(6)
Cu(1)	8h	0.2590(3)	0.2504(1)	0.2576(4)	1.0	0.073(1)	0.113(2)	0.0399(7)	0.066(2)	−0.0104(6)	−0.013(1)	−0.0197(6)
Cu(2)	4g	0.2712(3)	0.5102(3)	0	1.0	0.072(1)	0.093(2)	0.099(2)	0.0231(7)	0.066(2)	0	0
Cu(3)	8h	0.4936(2)	0.3467(3)	0.3794(10)	0.524(3)	0.091(1)	0.041(1)	0.082(2)	0.149(3)	0.012(2)	−0.043(2)	0.017(2)
Cu(4)	8h	0.0171(10)	0.0353(12)	0.2273(7)	0.476(3)	0.143(4)	0.046(3)	0.234(11)	0.149(3)	0.075(4)	−0.046(4)	−0.102(5)
					$T = -80\,^{\circ}C$							
I(1)	4g	0.55054(7)	0.26615(6)	0	1	0.0194(2)	0.0133(3)	0.0289(4)	0.0160(3)	0.0006(3)	0	0
I(2)	4g	0.08147(6)	0.63998(5)	0	1	0.0169(2)	0.0154(3)	0.0131(3)	0.0222(3)	0.0001(2)	0	0
Sb	4g	0.31107(6)	0.00655(5)	0	1	0.0130(2)	0.0095(3)	0.0133(3)	0.0161(3)	−0.0006(2)	0	0
S(1)	4g	0.1917(2)	0.1716(2)	0	1	0.0154(7)	0.013(1)	0.014(1)	0.019(1)	−0.0005(9)	0	0
S(2)	8h	0.3169(2)	0.4239(1)	0.2582(2)	1	0.0184(5)	0.0207(9)	0.0222(9)	0.0124(8)	0.0080(7)	−0.0008(7)	−0.0021(7)
Cu(1a)	8h	0.2525(8)	0.2413(9)	0.277(2)	0.56(6)	0.022(2)	0.033(3)	0.019(2)	0.014(3)	0.000(2)	−0.001(2)	0.000(2)
Cu(1b)	8h	0.255(5)	0.255(2)	0.244(5)	0.23(6)	0.045(9)	0.11(3)	0.012(5)	0.010(6)	−0.023(8)	0.009(5)	−0.004(4)
Cu(1c)	8h	0.335(1)	0.2534(7)	0.208(2)	0.20(1)	0.027(3)	0.032(5)	0.023(3)	0.027(5)	0.000(3)	−0.004(4)	−0.003(3)
Cu(2a)	4g	0.3031(8)	0.5383(7)	0	0.43(1)	0.026(2)	0.035(3)	0.025(3)	0.016(2)	0.010(3)	0	0
Cu(2b)	4g	0.2486(7)	0.4936(6)	0	0.56(2)	0.030(1)	0.044(3)	0.031(3)	0.014(1)	0.019(3)	0	0
Cu(3a)	8h	0.4988(3)	0.3455(3)	0.3671(5)	0.465(4)	0.059(1)	0.025(1)	0.088(3)	0.066(3)	0.016(1)	−0.014(1)	0.023(2)
Cu(3b)	4g	0.477(2)	0.364(2)	0.5	0.070(8)	0.029(9)	–	–	–	–		–
Cu(4a)	8h	0.0180(10)	0.0495(10)	0.222(2)	0.41(2)	0.071(3)	0.021(3)	0.074(6)	0.115(5)	0.022(3)	−0.015(3)	−0.025(3)
Cu(4b)	4e	0	0	0.246(2)	0.17(4)	0.09(2)	0.006(6)	0.26(5)	0.01(1)	−0.03(2)	0	0

[a] U_{eq} is defined as one third of the trace of the anisotropic U^{ij} tensor. The anisotropic displacement factor exponent takes the form $(-\pi^2\sum_i\sum_j U^{ij}|a_i^*||a_j^*|h_ih_j)$.

Table 3a. Selected interatomic distances [Å] and angles [°] for $(CuI)_2Cu_3SbS_3$ at 20 °C [a].

Sb–S(1)		2.434(2)	I(1)–Cu(1)*	2×	2.750(3)
Sb–S(2)	2×	2.446(2)	I(1)–Cu(3)*	2×	2.873(7)
Cu(1)*–S(1)		2.296(3)	I(2)–Cu(1)*	2×	2.785(3)
Cu(1)*–S(2)		2.318(2)	I(2)–Cu(2)*		2.570(4)
Cu(1)*–I(1)		2.750(3)	I(2)–Cu(3)*	2×	2.916(4)
Cu(1)*–I(2)		2.785(3)	S(1)–Sb		2.434(2)
Cu(2)*–S(2)	2×	2.208(2)	S(1)–Cu(1)*	2×	2.296(3)
Cu(2)*–I(2)		2.570(4)	S(1)–Cu(3)*	2×	2.285(4)
Cu(3)*–S(1)		2.285(4)	S(1)–Cu(4)*	2×	2.80(1)
Cu(3)*–S(2)		2.235(4)	S(2)–Sb		2.446(2)
Cu(3)*–I(1)		2.873(7)	S(2)–Cu(1)*		2.318(2)
Cu(3)*–I(2)		2.916(4)	S(2)–Cu(2)*		2.208(2)
Cu(4)*–S(1)		2.80(1)	S(2)–Cu(3)*		2.235(4)
Cu(4)*–S(2)		2.17(1)	S(2)–Cu(4)*		2.17(1)
Cu(4)*–S(2)		2.34(1)	S(2)–Cu(4)*		2.34(1)
S(1)-Sb-S(2)	2×	94.10(5)	I(1)-Cu(3)*-I(2)		93.90(13)
S(2)-Sb-S(2)		92.05(5)	I(1)-Cu(3)*-S(1)		101.4(1)
I(1)-Cu(1)*-I(2)		93.90(8)	I(1)-Cu(3)*-S(2)		91.3(2)
I(1)-Cu(1)*-S(1)		104.79(12)	I(2)-Cu(3)*-S(1)		89.7(2)
I(1)-Cu(1)*-S(2)		107.68(9)	I(2)-Cu(3)*-S(2)		106.66(10)
I(2)-Cu(1)*-S(1)		120.09(9)	S(1)-Cu(3)*-S(2)		158.7(2)
I(2)-Cu(1)*-S(2)		108.57(11)	S(1)-Cu(4)*-S(2)		87.6(3)
S(1)-Cu(1)*-S(2)		118.13(13)	S(1)-Cu(4)*-S(2)		126.2(5)
I(2)-Cu(2)*-S(2)	2×	119.59(8)	S(2)-Cu(4)*-S(2)		143.5(7)
S(2)-Cu(2)*-S(2)		118.6(2)			

[a] Atoms marked with an asterisk refer to the mode positions: Cu(1)* [0.2550(3), 0.2484(1), 0.2673(4)], Cu(2)* [0.2596(3), 0.5005(3), 0.], Cu(3)* [0.4947(2), 0.3464(3), 0.3597(10)], and Cu(4)* [0.0211(10), 0.0516(12), 0.2155(7)].

Table 3b. Selected interatomic distances [Å] for $(CuI)_2Cu_3SbS_3$ at −80 °C.

Cu(1a)–S(1)		2.29(1)	Cu(2b)–S(2)	2×	2.196(4)
Cu(1a)–S(2)		2.40(2)	Cu(2b)–I(2)		2.551(7)
Cu(1a)–I(1)		2.68(1)	Cu(3a)–S(1)		2.259(4)
Cu(1a)–I(2)		2.71(1)	Cu(3a)–S(2)		2.297(4)
Cu(1b)–S(1)		2.16(4)	Cu(3a)–I(1)		2.904(4)
Cu(1b)–S(2)		2.24(3)	Cu(3a)–I(2)		2.892(4)
Cu(1b)–I(1)		2.86(5)	Cu(3b)–S(1)		2.31(2)
Cu(1b)–I(2)		2.92(4)	Cu(3b)–S(2)	2×	2.55(2)
Cu(1c)–S(1)		2.37(1)	Cu(3b)–I(2)		2.89(2)
Cu(1c)–S(2)		2.189(9)	Cu(4a)–S(1)		2.89(1)
Cu(1c)–I(1)		2.74(2)	Cu(4a)–S(2)		2.15(1)
Cu(1c)–I(2)		2.71(1)	Cu(4a)–S(2)		2.36(1)
Cu(2a)–S(2)	2×	2.374(5)	Cu(4b)–S(2)	2×	2.154(2)
Cu(2a)–I(1)		2.908(8)			
Cu(2a)–I(2)		2.663(8)			

order Jahn–Teller effect;[11] that is the occupied nd and unoccupied $n+1$s orbitals are mixed. Such an effect is often observed in the crystal structures of d^{10} ions and becomes evident from the enlarged anisotropic displacement parameters of the corresponding atoms. This effect is most pronounced for Ag^+ and Cu^+ ions but is also detectable for Zn^{2+} and Cd^{2+} ions.[12] Large displacement parameters are also found for copper or silver atoms in several solid electrolytes, which exhibit an enhanced mobility for these atoms. Structure analyses at different temperatures should enable one to determine whether the large temperature parameters are due to nonharmonicity or ionic conductivity.[13]

A better refinement of the crystal structure at room temperature was obtained by using a Gram-Charlier development of the displacement parameters of the copper atoms up to fourth order to describe their distribution. Thus the number of copper positions was reduced to four, and only seven additional parameters had to be introduced in the refinement (tensor elements smaller than 3σ were fixed to zero[14]). The significance of the nonharmonic refinement was assessed from statistical tests.[15] Also, after introduction of the nonharmonic approach the highest peaks in the final difference Fourier calculation are observed close to the heaviest atoms; by contrast, for the split atom refinement they were still located near the much lighter copper atoms. This clearly indicates that the distribution of the copper

0947-6539/97/0312-2034 $ 17.50+.50/0 *Chem. Eur. J.* **1997**, *3*, No. 12

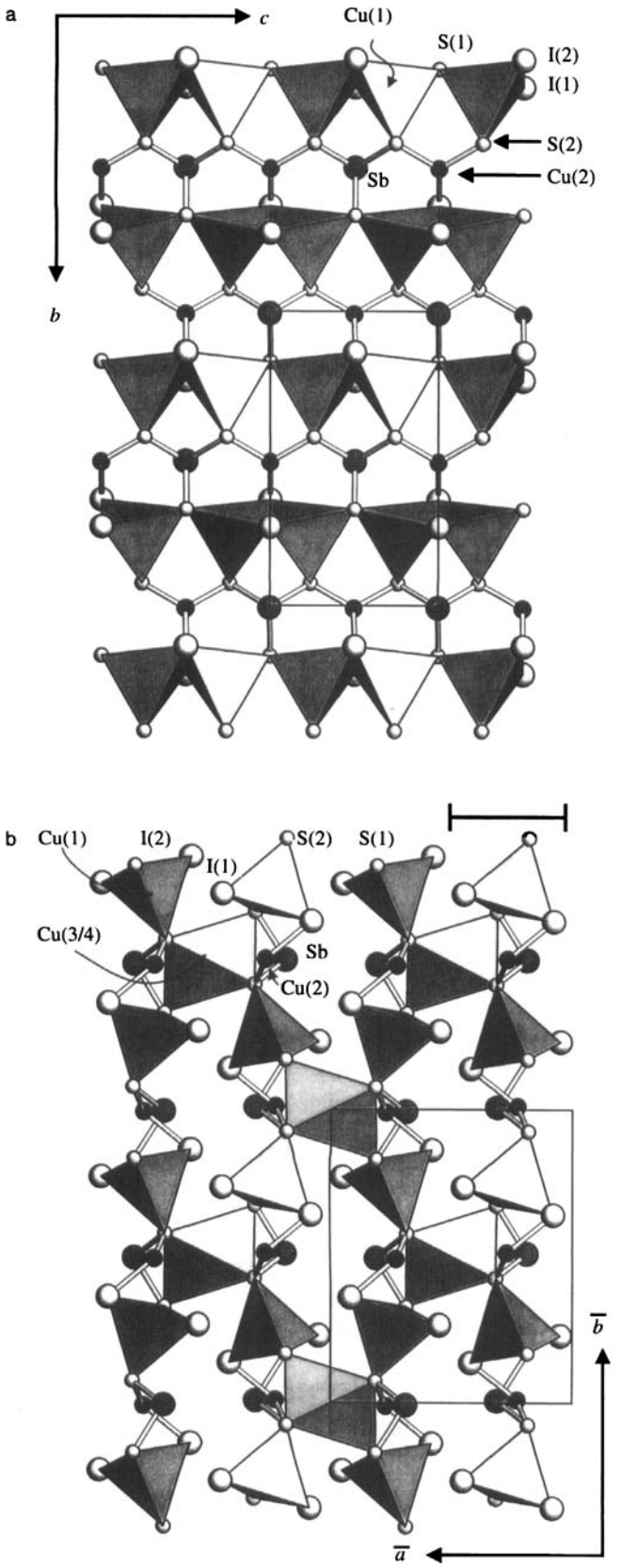

Figure 2. a) Section of the crystal structure of $(CuI)_2Cu_3SbS_3$ showing the ribbons parallel to [001] of tetrahedrally coordinated Cu(1) and those of trigonally coordinated Cu(2) and Sb, respectively. b) Connection of the layers shown in a) by S_6 octahedra. The copper atoms Cu(3) and Cu(4) (not shown explicitly) are distributed over the faces of these octahedra. The section shown in Figure 2a is marked by the horizontal bar. Cu: small black spheres; Sb: large dark spheres; S: small light gray spheres; I: large light gray spheres.

atoms is described in a better way by the nonharmonic approach. Another helpful tool to decide whether the results of a nonharmonic refinement are reasonable and significant is the probability density function (pdf), that is the Fourier transform of the displacement parameters, or in the case of overlapping pdfs the joint probability density function (jpdf), that is the sum of the weighted pdfs.[13] The pdf (or the jpdf) should show no significant negative regions. The jpdf for the copper atoms (Cu(3), Cu(4)) distributed around the above-mentioned S_6 octahedron, the nonharmonic deformation densities (pdf_{def}),[16] and the corresponding error map are shown in Figure 3. It becomes evident that the copper atoms are delocalized parallel to the *bc* plane, and the single pdfs overlap (for Cu(4)–Cu(4)′) or almost overlap (for Cu(3)–Cu(3)′ and Cu(3)–Cu(4)). A comparison of the values calculated for the pdf_{def} and the errors for the pdf indicate the significance of the refined model. Short distances d(Cu(3)–Cu(3)′) = 1.783(10), d(Cu(4)–Cu(4)′) = 0.95(2), and d(Cu(3)–Cu(4)) = 1.68(2) Å are calculated for the refined positions but of course they are meaningless since these two copper positions are occupied to only about 50%.

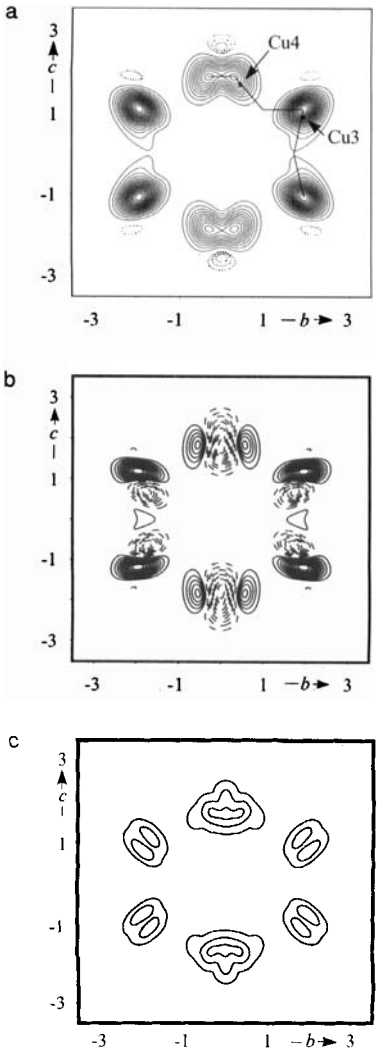

Figure 3. a) The pdf map (20 °C) of the copper atoms distributed around the faces of an S_6 octahedron: min./max. density: $-77/+2013$ Å^{-3}, step: $-20/+100$ Å^{-3}; b) the pdf_{def} map: min./max. deformation density: $-770/+480$ Å^{-3}, step $-80/+40$ Å^{-3}; c) the error of the pdf: max. 138 Å^{-3}, step + 40 Å^{-3}. The refined positions of Cu(3) and Cu(4) are indicated in Figure 3a.

  0947-6539/97/0312-2035 $ 17.50+.50/0

An effective one-particle-potential (opp), which provides some information for the potential barrier for the movement of a copper atom, can be derived from the jpdf. The opp along the zigzag line given in the jpdf map (Figure 3a) is shown in Figure 4. Two double minima (around the Cu(3) and the Cu(4) sites) and the strong deviations from a harmonic potential are visible.

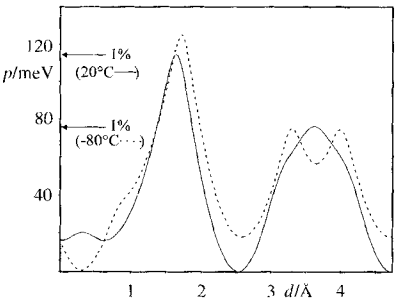

Figure 4. Effective opp along the line indicated in Figure 3a. At 20 °C a double minimum potential around both the sites of Cu(4) and Cu(4)′ and Cu(3) and Cu(3)′, respectively, is observed. At −80 °C the intermediate sites are also occupied and the potential around the Cu(4b) site becomes a single minimum potential. For the Cu(3) site a similar evolution becomes visible. The arrows indicate a cut-off of 1% according to Boltzmann statistics for the given temperatures.

Due to the height of the barrier between the positions of Cu(3) and Cu(4) (ca. 120 meV) one can assume a dynamic exchange between the eight maxima shown in Figure 3a, at least within a certain probability. Three-dimensional (3D) surface plots of the pdfs and jpdfs for the copper atoms in their coordination polyhedra of iodine and sulfur are presented in Figure 5. These plots indicate the pronounced deviations from a harmonic displacement of the corresponding atoms. For the copper atoms around the S_6 octahedron it becomes evident that owing to surrounding iodine atoms there are several tetrahedral voids available and copper is readily distributed in them.

For the dataset collected at −80 °C the nonharmonic refinement no longer works, instead the positions of the copper atoms can be resolved by using nine split positions for them. This is probably because of a stronger localization of the copper atoms, which is accompanied by an unusual temperature dependence of the lattice constants of the title compound; the length of the *a* axis increases when the crystals are cooled to −80 °C, whereas the *b* axis remains unchanged, and the *c* axis shortens. The main reason for this anisotropic temperature dependence of the lattice parameters is probably the nesting of copper atoms, especially around the above-mentioned S_6 octahedron. Details of the refinement of the dataset collected at −80 °C are compiled in Table 1 and atomic coordinates are given in Table 2. From the evolution of the potential curves (see Figure 4) with temperature it becomes evident that the copper atoms are mobile in $(CuI)_2Cu_3SbS_3$. As the temperature decreases, the intermediate sites, that is positions between the minima at 20 °C, become occupied. Thus, the double minimum curve for the Cu(4)/Cu(4)′ position at 20 °C changes to a single minimum curve at −80 °C, and the deviations from harmonicity are reminiscent of the potential curve at room temperature. For the potential curve at the Cu(3)/Cu(3)′ position the same tendency becomes evident. Since the coordination is different for Cu(3) and Cu(4) the effect is less pronounced for Cu(3). Particularly for the pair Cu(4a)/Cu(4b) (Cu(4a) corresponds to the position of Cu(4) at 20 °C) the lowering of the temperature results in a reduction of the coordination number from three to two; the S-Cu-S angle is 178.5(9)° for Cu(4b). This trend of reducing the coordination number also occurs for Cu(1) and Cu(2), which is evident from the distances given in Table 3b. The change of coordination numbers for Cu^+ and Ag^+ with temperature has been discussed, for example, in references [22, 23].

Raman spectroscopic investigations: According to Wang and Liebau[17] a change of the bonding properties of a lone pair atom can be best detected from changes in the bond angles, whereas bond lengths may remain almost unchanged. Thus interatomic *d*(Sb–S) distances are not very sensitive to the local environment of the antimony(III) ion. In the case of the title compound this effect is substantiated by Raman spectra. As already mentioned, the thioantimonate(III) ions $[SbS_3]^{3-}$ in $(CuI)_2Cu_3SbS_3$ can be regarded as separated from each other in the copper halide matrix and thus no additional sulfur atoms are observed as next-nearest neighbors for antimony. In contrast, in Cu_3SbS_3 (without the CuI matrix) antimony is surrounded by three + five sulfur atoms; the $\bar{d}$(Sb–S) distance for the three nearest S atoms is 2.465 Å (compared to $\bar{d}$(Sb–S) = 2.412 Å in $(CuI)_2Cu_3SbS_3$) and is 3.72 Å for the five next-nearest sulfur atoms (Figure 6).[24] The Raman spectra of $(CuI)_2Cu_3SbS_3$ and that of β-Cu_3SbS_3 (for comparison) are shown in Figure 7. Both spectra are dominated by strong bands for the $[SbS_3]^{3-}$ units. For the isolated thioantimonate(III) ion in the title compound vibrations are observed at 362 cm^{-1} and 339 cm^{-1}. According to spectroscopic data for $Sb(SR)_3$ ($R = C_4H_9, C_6H_5$) one would expect a band in the region between 365 and 380 cm^{-1} and a second one at about 340 cm^{-1}.[18] A strong shift of about 40 cm^{-1} for these two bands is observed for β-Cu_3SbS_3; the

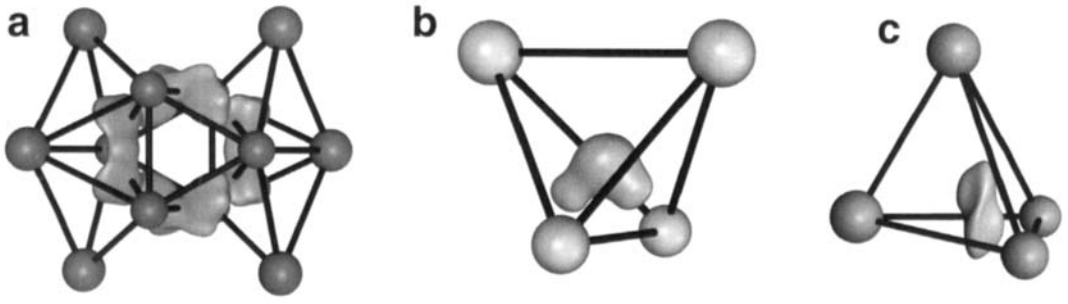

Figure 5. 3D surface plots (20 °C) for a) the jpdf of Cu(3) and Cu(4) around the S_6 octahedron in $(CuI)_2Cu_3SbS_3$ (S: small spheres, octahedron seen perpendicular to a sulfur triangle, I: large spheres completing the coordination of the copper atoms), b) the pdf of Cu(1) with tetrahedral coordination of two I and two S atoms, and c) the pdf of Cu(2) in a face of a tetrahedron built by two I and two S atoms.

0947-6539/97/0312-2036 $ 17.50+.50/0 Chem. Eur. J. 1997, 3, No. 12

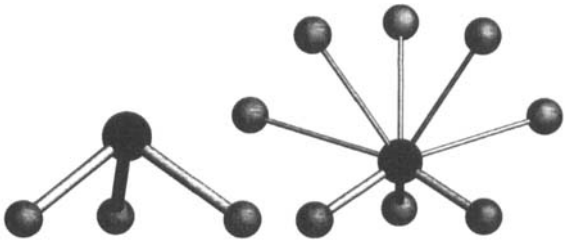

Figure 6. Coordination of antimony by three sulfur atoms in $(CuI)_2Cu_3SbS_3$ (left) and 3 + 5 sulfur atoms in β-Cu_3SbS_3 (right). Broad lines represent d(Sb–S) distances < 2.5 Å, thin lines indicate interatomic distances 2.5 Å < d(Sb–S) < 4 Å. The influence of the next-nearest sulfur atoms becomes visible from the change of the averaged S-Sb-S angle, which is 93.3° for the isolated $[SbS_3]^{3-}$ unit in $(CuI)_2Cu_3SbS_3$ and 98.6° for that in β-Cu_3SbS_3 (only for d(Sb–S) < 2.5 Å).

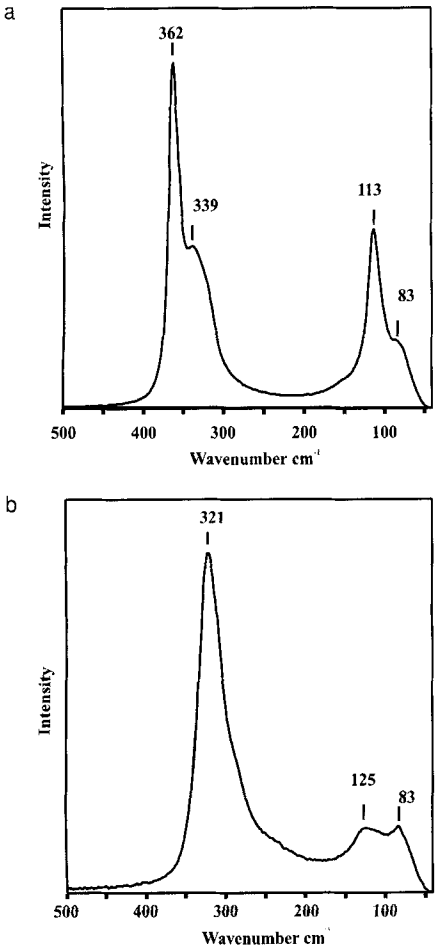

Figure 7. Raman spectra of a) $(CuI)_2Cu_3SbS_3$ and b) β-Cu_3SbS_3. Both spectra are dominated by the strong bands of the $[SbS_3]^{3-}$ units. Due to additional Sb–S interactions in β-Cu_3SbS_3 the corresponding bands are shifted to lower wavenumbers than in $(CuI)_2Cu_3SbS_3$. The weak band at 83 cm^{-1} is an experimental artifact.

corresponding maxima are found at 321 cm^{-1} and about 290 cm^{-1} (shoulder). The decreased bonding interactions within the $[SbS_3]^{3-}$ unit in β-Cu_3SbS_3 can be explained by the five next-nearest sulfur atoms.

Ionic conductivity: Based on the pronounced nonharmonic deformation of the pdf, a high ionic conductivity is expected for the copper atoms even at room temperature. Thus the impedance was measured to substantiate this assumption. Impedance spectra for $(CuI)_2Cu_3SbS_3$ between 30 °C and 280 °C show the typical shape for an ionic conductor contacted to blocking electrodes; that is, they consist of a linear spike at low frequencies and a semicircular arc at higher frequencies. The ionic conductivity can be extracted from these spectra. Selected conductivity values are $6.2 \times 10^{-5}\,\Omega^{-1}cm^{-1}$ (50 °C) and $2.9 \times 10^{-3}\,\Omega^{-1}cm^{-1}$ (200 °C), which are much higher than the corresponding data for pure CuI (e.g. ca. $10^{-5}\,\Omega^{-1}cm^{-1}$ (200 °C)[19]). The corresponding Arrhenius diagram is shown in Figure 8. The activation energy $E_A = 0.35$ eV is slightly higher than that of the good copper ion conductor $RbCu_4Cl_5$ ($E_A = 0.27$ eV),[19] whereas the absolute conductivity values are about one order of magnitude smaller at room temperature.

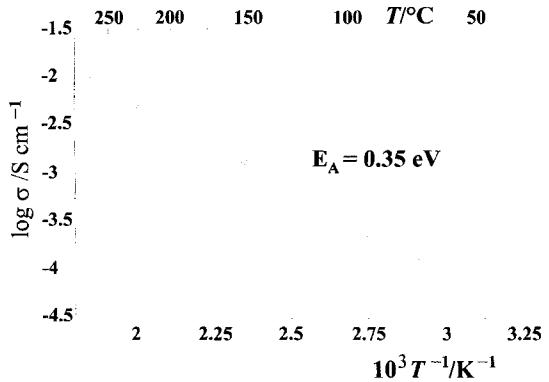

Figure 8. Temperature dependence of the ionic conductivity of $(CuI)_2Cu_3SbS_3$.

The conduction pathways of the copper atoms cannot be derived exactly from the X-ray structural data. A potential barrier similar to that obtained from the conductivity data should be visible from the nonharmonic refinement;[13, 20] however, for the given value of $E_A = 0.35$ eV a temperature of approximately 600 °C would be necessary to determine it within the 1% level according to Boltzmann statistics. At this temperature the compound is already molten.

Conclusion

Extension of the use of copper(I) halides as reaction media for the synthesis of new solid materials based not only on main group polymers but also on thiometalate ions has provided the compound $(CuI)_2Cu_3SbS_3$. The iodide ions in its crystal structure form an eutactic arrangement that is related to the hexagonal diamond structure. Inserted $[SbS_3]^{3-}$ units therein are isolated from each other, as is clearly demonstrated by Raman spectroscopic data. A pronounced temperature-dependent disorder of the copper atoms can be derived from X-ray structural investigations. At higher temperature the copper atoms tend to have a higher coordination number. Closely related to this, an enhanced copper ion conductivity is observed, which exceeds that of pure CuI by about two orders of magnitude.

Experimental Section

$(CuI)_2Cu_3SbS_3$ was prepared by reaction of stoichiometric amounts of CuI (powder, 99.999%, Aldrich), Cu (shot, m5N, Johnson Matthey), Sb (shot, 99.999%, Heraeus), and S (pieces, 99.999%, Fluka) (CuI:Cu:Sb:S =

  0947-6539/97/0312-2037 $ 17.50+.50/0

2:3:1:3) in evacuated silica ampoules. After heating the starting mixture to 500 °C for several hours it was homogenized by grinding. The compound was readily formed after six days at 430 °C. When the powder was kept at a temperature of 350 °C for three weeks a mixture of a phase pure red-orange micro-crystalline material and larger crystals suitable for an X-ray structure analysis were obtained. An alternative route that employed Cu_3SbS_3 and CuI as a flux medium was described in ref. [8]. The purity of the batch was checked by X-ray powder diffraction (SIEMENS D5000, $Cu_{K\alpha 1}$); the lattice constants were consistent with the single-crystal data within their esds. DTA measurements (LINSEIS L62) showed only one endothermal effect at 492 °C, which was assigned to the melting point. Single crystals of suitable size were selected for X-ray structure analyses at −80 and 20 °C. The crystals were fixed on top of a glass capillary and mounted on a four-circle diffractometer (NONIUS CAD4) equipped with a nitrogen cooling device. Crystallographic data are collected in Table 1. Since the copper atoms in $(CuI)_2Cu_3SbS_3$ are disordered over several positions a Gram-Charlier expansion[21] of the atomic displacement parameters was used to describe their distribution at room temperature. The significance of the obtained results for the pdf was checked by an analysis of its errors using a Monte–Carlo method[16] implemented in JANA96.[19, 22]

Ionic conductivity data were obtained from impedance spectra recorded with an IM6 impedance measurement unit (Zahner-Elektrik) in the frequency range from 100 mHz to 4 MHz. Cold pressed pellets (8 mm diameter; thickness 1–2 mm) contacted to gold electrodes were used for the measurements. Details for the experimental setup are given elsewhere.[6]

Raman spectra of $(CuI)_2Cu_3SbS_3$ (and for comparison of β-Cu_3SbS_3[24, 25]) were measured in a backscattering mode on a BRUKER RFS100/S using a Nd:YAG laser with an excitation wavelength of 1064 nm.

Acknowledgments: The author is grateful to Prof. Deiseroth for his continuous support and to T. Nilges and S. Reiser for help with the experiments. He also thanks Prof. Lutz for the use of his Raman spectrometer; spectra were recorded by R. Stötzel. This work was financially supported by the Deutsche Forschungsgemeinschaft.

Received: May 15, 1997 [F695]

[1] For example, M. G. Kanatzidis, A. C. Sutorik, *Prog. Inorg. Chem.* **1995**, *43*, 151; M. A. Pell, J. A. Ibers, *Chem. Ber.* **1997**, *130*, 1.
[2] A. Rabenau, *Angew. Chem.* **1985**, *97*, 1017; *Angew. Chem. Int. Ed. Engl.* **1985**, *24*, 1026.
[3] G. W. Drake, J. W. Kolis, *Coord. Chem. Rev.* **1994**, *137*, 131; W. S. Sheldrick, M. Wachhold, *Angew. Chem.* **1997**, *109*, 215; *Angew. Chem. Int. Ed. Engl.* **1997**, *36*, 206.
[4] For example, W. Milius, *Z. Anorg. Allg. Chem.* **1990**, *586*, 175; W. Milius, A. Rabenau, *Z. Naturforsch. B* **1988**, *43*, 243; A. Pfitzner, S. Zimmerer, *Z. Anorg. Allg. Chem.* **1995**, *621*, 969; *ibid.* **1996**, *622*, 853.
[5] H. M. Haendler, P. M. Carkner, S. M. Boudreau, R. A. Boudreau, *J. Solid State Chem.* **1979**, *29*, 35; W. Milius, A. Rabenau, *Mater. Res. Bull.* **1987**, *22*, 1493; A. Pfitzner, S. Zimmerer, *Z. Kristallogr.* **1997**, *212*, 203.
[6] M. H. Möller, W. Jeitschko, *J. Solid State Chem.* **1986**, *65*, 178; A. Pfitzner, E. Freudenthaler, *Angew. Chem.* **1995**, *107*, 1784; *Angew. Chem. Int. Ed. Engl.* **1995**, *34*, 1647; A. Pfitzner, E. Freudenthaler, *Z. Naturforsch. B* **1997**, *52*, 199; A. Pfitzner, E. Freudenthaler, *Z. Kristallogr.* **1995**, *210*, 59; E. Freudenthaler, A. Pfitzner, *ibid.* **1997**, *212*, 103; E. Freudenthaler, A. Pfitzner, *Solid State Ionics*, in press.
[7] A. Pfitzner, S. Zimmerer, *Angew. Chem.* **1997**, *109*, 1031; *Angew. Chem. Int. Ed. Engl.* **1997**, *36*, 982.
[8] T. J. Bastow, H. J. Whitfield, *J. Solid State Chem.* **1981**, *40*, 203.
[9] V. Petricek, JANA96, Institute of Physics, Academy of Sciences of the Czech Republic, Prague, Czech Republic **1996**.
[10] P. J. Becker, P. Coppens. *Acta Cryst. Sect. A* **1974**, *30*, 129.
[11] J. K. Burdett, O. Eisenstein, *Inorg. Chem.* **1992**, *31*, 1758.
[12] F. Boucher, M. Evain, R. Brec, *J. Alloy Compd.* **1994**, *215*, 63.
[13] R. Bachmann, H. Schulz, *Acta Crystallogr. Sect. A* **1984**, *40*, 668.
[14] W. F. Kuhs, *Acta Crystallogr. Sect. A* **1983**, *39*, 148.
[15] W. C. Hamilton, *Acta Crystallogr.* **1965**, *18*, 502.
[16] W. F. Kuhs, *Acta Crystallogr. Sect. A* **1992**, *48*, 80.
[17] X. Wang, F. Liebau, *Acta Crystallogr. Sect. B* **1996**, *52*, 7; X. Wang, F. Liebau, *Z. Kristallogr.* **1996**, *211*, 437.
[18] J. Weidlein, U. Müller, K. Dehnicke, *Schwingungsfrequenzen I*, Thieme, Stuttgart, **1981**, p. 155.
[19] T. Matsui, J. B. Wagner Jr., *J. Electrochem. Soc.* **1977**, *124*, 937.
[20] U. H. Zucker, H. Schulz, *Acta Crystallogr. Sect. A* **1982**, *38*, 568.
[21] C. K. Johnson, H. A. Levy in *International Tables for X-ray Crystallography, Vol. IV* (Eds.: J. A. Ibers, W. C. Hamilton), Kynoch Press, Birmingham, **1974**, pp. 311–336.
[22] A. Pfitzner, M. Evain, V. Petricek, *Acta Crystallogr. Sect. B* **1997**, *53*, 337.
[23] A. van der Lee, F. Boucher, M. Evain, R. Brec, *Z. Kristallogr.* **1993**, *203*, 247.
[24] A. Pfitzner, *Z. Anorg. Allg. Chem.* **1994**, *620*, 1992.
[25] E. Makovicky, T. Balic-Zunic, *Can. Mineral.* **1995**, *33*, 655.

  0947-6539/97/0312-2038 $ 17.50+.50/0